Research Repository UCD

Title	Electric Field-Driven Catalytic Activity Using a Bioinspired Peptide and Titanium Dioxide Semiconductor Composite with Metal Nanoparticles
Authors(s)	Almohammed, Sawsan, Fularz, Agata, Rodriguez, Brian J., Rice, James H.
Publication date	2020-11-24
Publication information	Almohammed, Sawsan, Agata Fularz, Brian J. Rodriguez, and James H. Rice. "Electric Field-Driven Catalytic Activity Using a Bioinspired Peptide and Titanium Dioxide Semiconductor Composite with Metal Nanoparticles." American Chemical Society, November 24, 2020. https://doi.org/10.1021/acs.jpcc.0c08824.
Publisher	American Chemical Society
Item record/more information	http://hdl.handle.net/10197/11996
Publisher's statement	This document is the Accepted Manuscript version of a Published Work that appeared in final form in The Journal of Physical Chemistry C, copyright © 2020 American Chemical Society after peer review and technical editing by the publisher. To access the final edited and published work see http://pubs.acs.org/doi/abs/10.1021/acs.jpcc.0c08824.
Publisher's version (DOI)	10.1021/acs.jpcc.0c08824

Downloaded 2026-05-01 23:34:03

The UCD community has made this article openly available. Please share how this access benefits you. Your story matters! (@ucd_oa)

© Some rights reserved. For more information

Electric field-driven catalytic activity using a bioinspired peptide and titanium dioxide semiconductor composite with metal nanoparticles

Sawsan Almohammed [a, b], Agata Fularz [a], Brian J. Rodriguez * [a,b], and James H. Rice * [a]

[a]*School of Physics, University College Dublin, Belfield, Dublin 4, Ireland*
[b]*Conway Institute of Biomolecular and Biomedical Research, University College Dublin, Belfield, Dublin 4, Ireland*

Abstract
Heterogeneous catalytic processes facilitated by the localized surface plasmon resonance excitation in plasmonic nanomaterials possess the potential to increase product yield and selectivity in a range of redox reactions beyond what is possible when using traditional catalysis-based approaches. In this article, we demonstrate electric field (that was generated by applying DC voltage) driven redox catalysis (with and without UV irradiation) using plasmonic nanoparticles with a peptide nanotube/titanium dioxide hybrid semiconductor nanocomposite. The applied DC voltage reduces the bandgap of the peptide nanotubes, enabling control over the semiconductor–metal charge transfer rate. In the presence of the electric field, product formation from the hybrid semiconductor nanocomposite was c.a. 5 times faster than when using peptide nanotubes or titanium dioxide alone. The product formation was further enhanced in combination with UV irradiation with an overall 9-fold enhancement.

Introduction

Heterogeneous catalytic processes facilitated by the localized surface plasmon resonance (LSPR) excitation in plasmonic nanomaterials have been studied intensively.[1–4] However, due to the rapid relaxation of hot carriers on femto- to picosecond timescales in plasmonic metal nanoparticle (NP)-based substrates, the path of LSPR-catalyzed reactions remains difficult to control.[1–4] One charge transfer route to control the charge state in the metal NPs is to include semiconducting nanomaterials such as titanium dioxide (TiO_2) NPs.[5] The oxidation of *p*-aminothiophenol (PATP) to 4,4'-dimercaptoazobenzene (DMAB) is a well-studied LSPR-mediated catalytic reaction.[5,6] Controlling the charge state in the metal NP with TiO_2 offers an effective route to control the plasmonic redox reaction rate.[5] Recently, the LSPR-mediated oxidation of PATP by gold (Au) NPs has been tuned by controlling the charge state on the metal though charge transfer from photoexcited TiO_2 to Au.[5–10] The LSPR-mediated oxidation of PATP in Au NPs leads to the formation of DMAB and the use of TiO_2-Au NPs under both super bandgap (UV) and LSPR excitation reportedly leads to a one-step oxidation of PATP to PNTP.[5,9,10] Additionally, PNTP could be further reduced to DMAB on the TiO_2-Au NPs when the UV-excitation was turned off.

Organic semiconductor self-assembled materials offer an alternative to the more traditionally used semiconductor materials such as TiO_2.[11–15] Diphenylalanine peptide nanotubes (PNTs) possess high thermal stability,[16] ease of preparation,[15,17–19] a wide bandgap (E_g ~ 4.6 eV),[20–22] and ability to bind with metal ions at specific locations.[23–26] PNTs have been shown to enhance the photoluminescent properties of photosensitizer molecules via a cascaded energy transfer

process[27] and to mediate the energy transfer from photoexcited molecules or chromophores to catalytic centers.[27,28] Here, we examine electric field-driven catalytic activity using a combination of TiO_2 nanotubes (TNTs) and peptide nanotube semiconductors with plasmonic metal NPs. We show that the use of an external electric field in combination with super bandgap UV irradiation leads to an increased reaction rate for PATP ↔ PNTP relative to using UV irradiation or applied electric field alone. Additionally, a higher reaction yield was found when the PNTs were combined with TNTs, compared to each separately in the presence of plasmonic metal NPs.

Materials and methods

Template formation

PNTs were formed by dissolving L-diphenylalanine peptide (Bachem) in 1,1,1,3,3,3-hexafluoro-2-propanol (Sigma-Aldrich). The starting concentration of 100 mg ml^{-1} was then diluted in deionized water to a final concentration of 2 mg ml^{-1}. Solutions of TNTs were prepared by mixing dry TNTs with deionized water to a concentration of 10^{-3} M and sonicating for 30 minutes. The process is illustrated in Figure 1(a-c). The PNTs:TNTs templates were prepared by mixing PNTs:TNTs at different ratios (1:1, 1:2, and 1:3) upon heating and stirring at ~ 100 °C for 10–15 minutes. When AgNPs (0.02 mg ml^{-1}) were used, they were added to the mixture of PNTs and TNTs during the heating process, as illustrated in Figure 1(d-f).

Following this, 40 µl of the mixed solution was then placed on the gold electrode patterned silicon substrate to create the PNTs:TNTs-AgNP template (Figure 1(c)). For the control sample, AgNPs with and without TNTs on a silicon substrate were prepared using AgNPs (0.02 mg ml^{-1}), which were diluted to match the concentration used previously. Then, 40 µl of the solution was deposited on the silicon substrate for comparison.

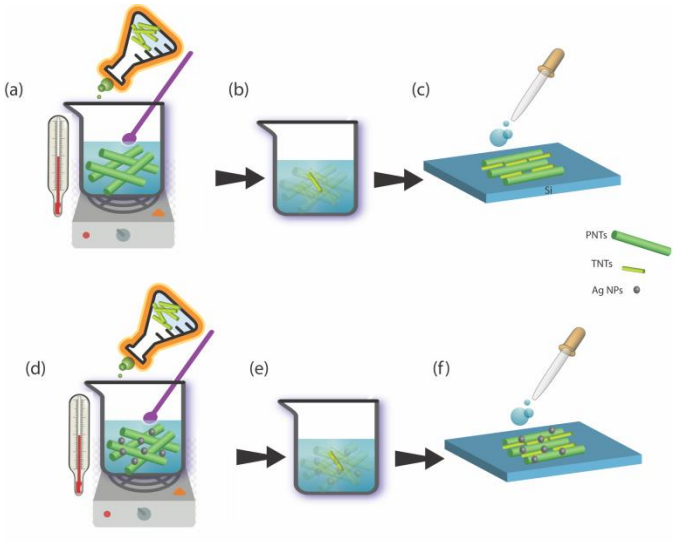

Figure 1. (a-f) Schematic illustration of the process to form PNTs:TNTs nanocomposites with and without AgNPs.

Preparation of the silicon substrate with a gold electrode pair

Silicon wafers (Si Mat) were cut as 2 cm × 1 cm samples. To make the gold electrode pair on the silicon substrate, a 3D printed mask with dimensions of 2 cm × 1 cm and 1 mm openings was used (Figure 2(a)). Gold was sputtered through mask openings to form the electrode pair. To make a wettability difference on the microfabricated chip device, UV ozone was used to form an oxide layer (SiO_2). More details on the overall process can be found in a previous publication.[29]

Probe molecule solution

4-Aminothiophenol (PATP) (New Star Chemical) solutions were prepared in methanol to a concentration of 10^{-4} M. This solution was then diluted with deionized water to final concentrations of 10^{-5} and 10^{-10} M. 4-Nitrophenol solution (PNTP) (N7660, Sigma-Aldrich Ireland) was diluted with deionized water to final concentrations of 10^{-4} and 10^{-6} M.

Spectral characterization

Optical absorbance measurements (V-650, JASCO, Inc.) were undertaken using a 1 nm step size with a 1 nm bandwidth and a 400 nm min^{-1} scan speed. The spectra were recorded over a wavelength range of 190–900 nm.

Scanning electron microscopy (SEM) (JSM-7600F). To obtain the SEM images, a thin (~ 10 nm) layer of gold was sputtered on the samples before imaging (Hummer IV, Anatech USA).

Raman and surface enhanced Raman spectroscopy. In order to record SERS spectra, a bespoke Raman system was employed. This system consists of an inverted optical microscope (IX71) with a SP-2300i spectrograph (Princeton Instruments), and a CCD camera (IXON). The 532 nm Raman excitation wavelength was fixed at a 5 mW incident laser power. SERS measurements were performed in the presence of electric field (a DC power supply (TENMA, 72–2015)) with voltages in the range of 5–60 V, resulting in an electric field strength of 5–60 V/mm. During SERS measurements, the voltage was applied across the electrode pair on either side of the PNTs:TNTs template with and without AgNPs and the probe molecule. The UV irradiation was applied using a UV pencil lamp with wavelength of 254 nm and a nominal output power of 4.5 mW cm^{-2} (Edmond Optics) located approximately 2 cm from the PNTs:TNTs-AgNP template with and without the probe molecule.

Results and discussion

The microfabricated device was prepared following the process reported previously.[1,22] Briefly, composites of PNTs and TNTs (PNTs:TNTs) were prepared with and without silver nanoparticles (AgNPs). The composites were deposited between microfabricated gold electrodes with a gap of ~ 1000 μm between electrode pairs on a silicon substrate. The silicon substrate was prepared with a silicon dioxide surface layer prior to the deposition of the electrodes and PNTs:TNTs. The composite forms an aligned arrangement of PNTs between the electrodes, as shown schematically in Figure 2(a). Such an ordering of PNT-based composites has been previously noted when using PNTs with AgNPs or graphene based nanomaterials.[29,30]

The PNTs:TNTs composites were prepared at different ratios to investigate the influence of TNTs on the PNT formation and alignment. Optical microscopy and scanning electron microscopy (SEM) were used to characterize the topology/morphology of the composite

templates (Figures 2(b) and S1–S5). As the amount of TNTs increased, the PNTs became shorter and thinner, reduced from 3.2 ± 1.3 μm to 0.6 ± 0.8 μm in width. A further increase in the amount of TNTs resulted in flower-like structures (Figures 2(b), S1 and S2). Inspection of the microscopy images shows that TNTs form nanostructures with diameters of around 100 nm in the presence or absence of PNTs and that the alignment of the PNTs was optimum when PNTs:TNTs ratios of 1:1 or 1:2 were used (Figures S3–S5).

The electrical properties of the composite were then studied. The current measured through the PNTs:TNTs template as a function of applied voltage shows Ohmic behavior (Figure 2(c)), with a lower resistance (375 ± 1 Ω for 1:1 ratio) (Figure 2(c)) than for AgNPs (1583 ± 1 Ω) or PNTs (930 ± 1 Ω) alone.[31] The absorption spectrum for PNTs alone is transparent over the visible range with absorption peaks at ~ 222 nm and ~ 260 nm, due to π–π* electronic transitions of the phenyl group in the PNTs (Figure S6), in agreement with previous reports.[29,30] In combined PNTs-AgNPs, the SPR band arising from AgNPs appeared at ~ 430 nm This is in agreement with studies reporting that amino acid carboxyl groups bind to metal NPs, which results in a red shift in the SPR absorption band.[32]

Bandgap calculations from optical absorption spectra (Figures 2(d) and S7) of the composites reveals a reduction in the bandgap from 4.4 $\pm$ 0.2 eV for PNTs to 4.0 $\pm$ 0.1 eV for PNTs:TNTs. Such a reduction in bandgap energy is a strong indication that the PNTs and TNTs structures are in close proximity and that their electronic states are interacting. Since both conductivity and alignment are best for a PNTs:TNTs ratio of 1:1, we have used it in the current study. Studies were performed to assess the stability of the PNTs:TNTs composite following the addition of an aqueous solvent, required to add target molecules for catalysis. The PNTs:TNTs template was found to be stable after the addition of the solvent, as shown through SEM imaging (Figure S8).

We have investigated the redox reaction PATP ↔ PNTP using the PNTs:TNTs-AgNP template. The SERS spectrum of PATP on the template prior to the application of super bandgap irradiation or an applied electric field (generated as a voltage is applied between two electrodes with ~ 1000 μm spacing with field strength varying between 0 and 50 V/mm depending on the voltage applied) shows strong b_2 Raman bands located at 1432, 1390, 1144, and 1076 cm^{-1} along with 1088 and 1594 cm^{-1} a_1 Raman bands (Figure S9). These Raman bands are assigned to the dimerization of PATP on the AgNPs to form DMAB.[32] As control studies, Raman measurements were performed for PATP and commercial PNTP with and without metal NPs for comparison (Figure S9).

Super bandgap energy irradiation of the template in the presence and absence of PNTs with PATP was undertaken using an irradiation source at 4.8 eV (λ_{ex} ~ 260 nm; Figures S10–S12). Following irradiation, the SERS spectrum showed the formation of new Raman bands, characteristic of the formation of PNTP,[5–7] at 1333 and 1632 cm^{-1}, which were not present before irradiation. The Raman band at 1333 cm^{-1} is assigned to a nitro symmetric stretching mode (NO_2) and the 1632 cm^{-1} Raman band is assigned to an amine scissoring mode (NH_2).[5–7] The results demonstrate that super bandgap irradiation facilitates the oxidation of PATP to form PNTP. Sub bandgap energy irradiation has been shown to be insufficient to excite electrons from PNTs.[32,33]

Raman measurements were then undertaken in the presence of an applied electric field Figure 2(e)). When subjecting the template to an electric field of 20 V/mm, new Raman bands at 1333 and 1632 cm^{-1} appear. These two Raman bands increase linearly in intensity as the applied voltage increases from 10 to 25 V. These two bands are characteristic of the formation of PNTP.[5–7] This demonstrates that an applied electric field effectively supports the oxidation reaction PATP ⟷ PNTP. It has been reported previously that PATP deposited on AgNPs results in dimerization and the production of a new compound called p,p'- dimercaptoazobenzene (DMAB). In such a process the amino groups (-NH_2) of two PATP molecules are oxidized and become azo bound (N=N bond is created). The SERS spectra of DMAB have peaks at 1432 and 1390 cm^{-1}, which are assigned to the stretching vibration of N=N (ν(N=N)) and a band located at 1144 cm^{-1} that is assigned to CH bending vibration (β(CH)). The intensities of these bands are enhanced with electric field, indicating the possibility of charge transfer between the template and the probe molecule PATP that further enhance the oxidation reaction.[32,34]

Combining super bandgap UV and electric field together further strengthens the Raman intensities of the two PNTP peaks at 1333 and 1632 cm^{-1} with respect to the DMAB peak intensities (Figure 3(a)), driving the redox reaction more effectively with respect to using the electric field or super bandgap UV irradiation alone (Figure 3(a)). Removal of the electric field and super bandgap UV irradiation causes the reaction to reverse with DMAB reformed. This coincides with the loss of the characteristic Raman bands for PNTP in the SERS spectrum (Figure 3(b)). Reintroduction of the electric field and UV irradiation reforms PNTP, demonstrating the reversibility of the reaction (Figure 3(b)). As a control, SERS measurements were performed for PATP on PNTs:TNTs only, in the absence of AgNPs (Figure S13).

Plotting the SERS intensity as a function of the applied electric field for a PNTP specific Raman band at 1333 cm^{-1} (Figure 3(c)) shows that the SERS signal intensity for this band increases as the applied voltage increases up to 25 V with and without UV irradiation. Such an enhanced catalytic behavior could be attributed to improved electron conductivity, metal dispersion, and reactive site exposure as previously reported for peptide-templated noble metal catalysts.[33] It should be noted that a resonance effect arising from AgNPs with the laser excitation wavelength (532 nm) also is unlikely to play a role in the overall enhancement observed in our case since light absorption by the PNTs-AgNPs is weak (Figure S6). Increasing the applied voltage higher than 25 V results in a continuous decrease in the Raman band intensity with and without UV irradiation (Figure 3(c)). Relaxation was also recorded after removing the electric field and UV as a function of time after removal (Figure S14). It can be clearly seen that both the product formation and SERS intensity will relax back to their original state after approximately 60 minutes, depending on the applied DC voltage and UV irradiation.

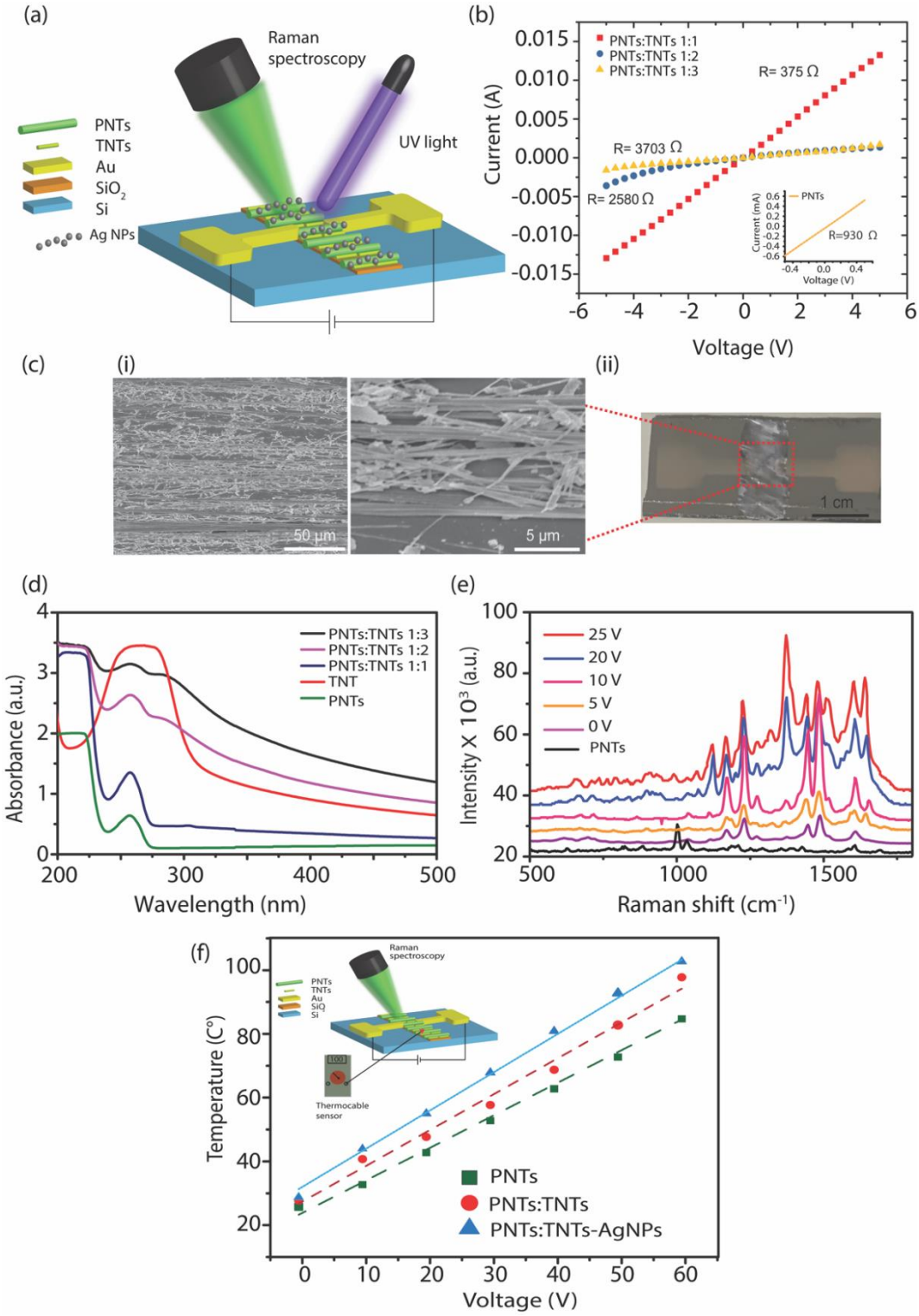

Figure 2. (a) Schematic illustration of microfabricated chip design. **(b)** IV measurement of the composite structures**. (c)** (i) SEM images of a PNTs:TNTs template and (ii) microfabricated chip design after depositing the PNTs and TNTs with AgNPs, dried at room temperature. **(d)** UV–vis measurement of PNTs with and without TNTs. **(e)** SERS monitoring of the redox reaction PATP ↔ PNTP on a PNTs:TNTs-AgNP template. Applying a DC voltage to the substrate over a range of 0 to 25 V. **(f)** Evolution of the temperature of the PNTs:TNTs-AgNP template with increasing DC voltage from 0 to 60 V.

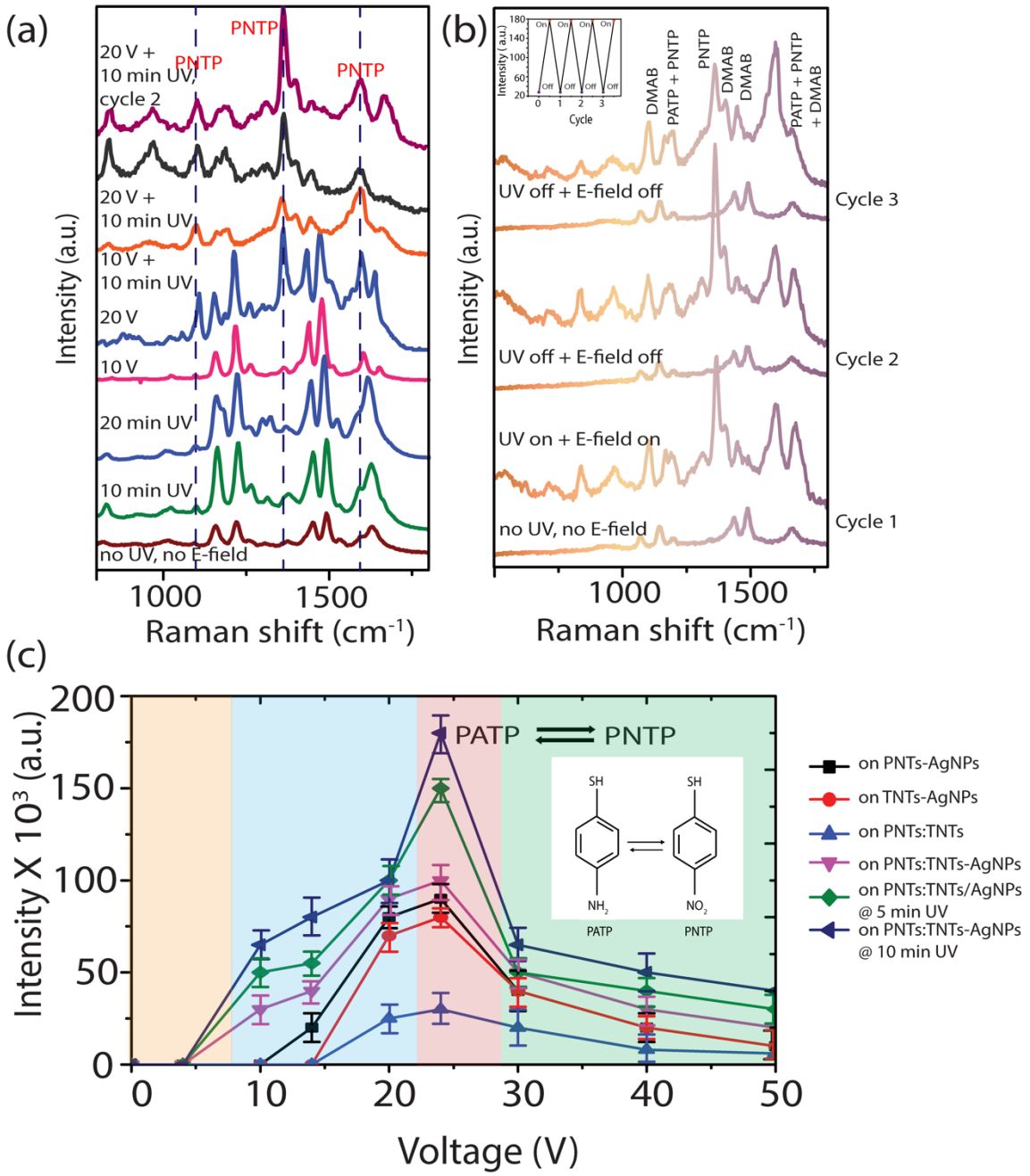

Figure 3. (a) SERS spectra of the redox reaction PATP ↔ PNTP on the PNTs:TNTs-AgNP template using UV irradiation or electric field stimulation or a combination thereof. The black and purple spectra show the signal obtained from 20 V and 10 minutes of UV irradiation before in the first and second instance (cycle 2). **(b)** SERS spectra showing the reversibility of the redox reaction PATP ↔ PNTP. The inset in (b) is the intensity of the product formation band at 1333 cm^{-1} at different cycles when DC voltage and UV irradiation are on and off. **(c)** Plot of SERS intensity as a function of the applied electric field with and without UV irradiation on PNTs:TNTs templates with and without AgNPs for the band at 1333 cm^{-1} associated with PNTP. Orange shading indicates a region with PNTP. Blue shading indicates the onset of the PATP to PNTP transformation. Red shading indicates the region of highest PNTP yield. Green shading shows a reduction in the formation of PNTP with higher voltages applied. The inset in (c) shows the chemical structure of PATP and PNTP.

It is reported that thermal effects can contribute to plasmonic catalysis reaction rates.[34] Thermal measurements of the substrate under an applied electric field show that as the applied voltage increases, the substrate temperature increases (Figure 2(f)). The maximum PNTP yield occurs at c.a. 25 V, which corresponds to a substrate temperature of c.a. 60 °C. The application of higher voltages, resulting in higher temperatures, coincides with reduced PNTP yield. The reduction in SERS intensity when the voltage exceeded 25 V could be associated with the pyroelectricity of PNTs.[20,35] The increased temperature arising from the applied voltage could lead to enhanced charge transfer from PNTs to TNTs and AgNPs up to ~ 60 °C.[36] As expected, the SERS intensity decreased for voltages > ~ 25 V (Figures 2(f) and 2(c)), as the temperature reached ~ 100 °C.

Studies of PNTs have shown that thermally induced water loss corresponds to changes in the chemical and hydrogen bonds that hold the PNT structure together.[35] The presence of water molecules has been shown to enhance the conductivity of PNTs, while evaporation of water reportedly disturbed dipole ordering in the PNT nanochannels (Figure S15) and led to irreversibly reduced conductivity, SERS signal, and photocatalyst activity.[20,35] In contrast, the electric field induced enhancement demonstrated here is cyclable (Figure 3(b)), allowing repeated control over PNTP yield, suggesting that evaporation of water during heating is not a primary mechanism of the observed behavior. Furthermore, we have previously demonstrated theoretically that upon increasing the electric field strength, the PNTs yield first conducting and then insulating behavior, and that an optimum applied field strength is required to maximize the conducting and catalytic behavior.[37] These findings suggest there is also an optimal applied field strength with respect to maximizing PNTP product formation, as explained below.

The impact of the TNTs is seen when looking at the onset of PNTP product formation. An applied field of 10 V is required using the PNTs:TNTs-AgNP template (Figures 3(c) and S12) in order to begin to form PNTP. In this sample at 10 V the 1333 cm^{-1} Raman band appears and gains intensity with increasing electric field strength. This compares to a requirement that an electric field strength of 15 V/mm be applied when using PNTs-AgNPs in the absence of TNTs. Also, 5–10 min of super bandgap UV irradiation is needed to drive the chemical transformation of PATP to PNTP when TNTs are present with PNTs-AgNPs, in comparison to 45 min when using PNTs-AgNPs only.[32] This demonstrates that the PNTs:TNTs-Ag-NP template produces a faster transformation of PATP to PNTP compared to when using PNTs-AgNPs in the absence of TNTs.

The band energies for each of the template's material components (e.g., AgNPs, PNTs, and TNTs) are outlined schematically in Figure 4. We have previously determined the work function of PNTs to be ~ 6.2 eV using Kelvin probe force microscopy.[32] The reported electron affinity (conduction band minimum) value of diphenylalanine PNTs is ~ 4.4 eV.[29,37] TiO_2 is a well-known wide bandgap (3.2 eV) semiconductor with its conduction band minimum located 4.0 eV below the vacuum level.[38] The reported value of the work function of TiO_2 varies by up to 1 eV depending on the crystal orientation,[39] with values between 4.2 to 4.9 eV reported.[38,40] Here, a value of 4.4 eV[41] was assumed. The work function of Ag (E_{FAg} = 4.26 eV) is lower than that of TiO_2, which results in the formation of an Ohmic contact between the two materials (Figure 4).[38] Electrons can be excited in both TNTs and PNTs using a super bandgap UV irradiation light source (λ_{ex} = 254 nm; 4.8 eV). Electrons flow from PNTs to TNTs

and then to AgNPs because of the difference in the Fermi level values ($E_{F,PNTs} > E_{F,TNTs} > E_{F,Ag}$).[40] The electrons accumulated on the AgNPs can be excited by either the green Raman excitation laser (532 nm; 2.3 eV) or the super bandgap UV light and transferred to the lowest unoccupied molecular orbital of PATP. The application of an external electric field reduces the bandgap in PNTs, and potentially also in TNTs, enhancing the rate and efficiency of this process.[42] The charge from the template is transferred to the lowest occupied molecule orbital of the PATP molecule weakening the resonance structure in line with the work functions for these systems (Figure 4). Vibrational modes that are sensitive to this resonance structure, will be downshifted. Specifically, these are the C=C stretching 1595 cm^{-1} and the C–S stretching 1082 cm^{-1} peaks for PATP. The shift in the frequency can be understood as due to the strong interaction between the analyte molecule and substrate. Such behavior of PATP and the downshifts in the bands was previously observed when using other substrate design such as TNTs with metal NPs.[1–3,5] When voltage > 30 V is applied, the bandgap of the PNTs is predicted to get larger reducing the efficiency of charge transfer based processes.[29,37]

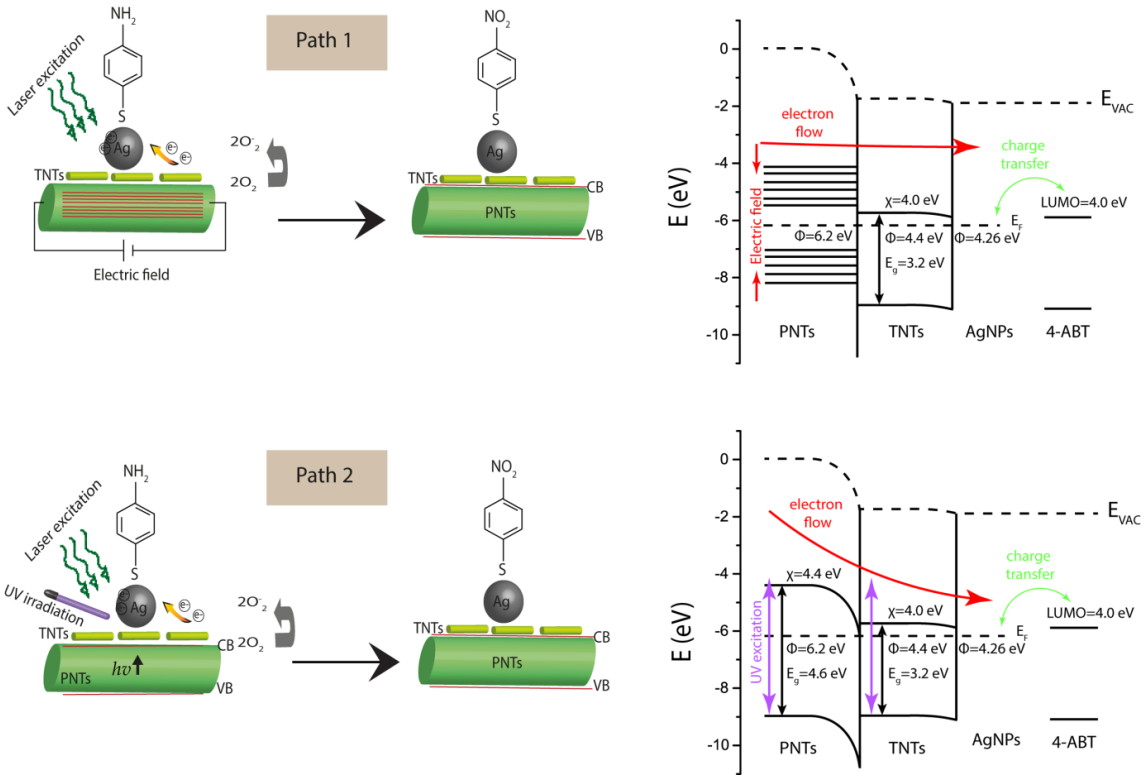

Figure 4. Schematic illustration of the possible photocatalyst process occurring when electric field (Path 1) or UV irradiation (Path 2) is applied. Band diagrams (right) illustrating the charge transfer between PNTs:TNTs-AgNPs and probe molecule PATP with electric field or UV irradiation.

Conclusions

Our results show that the PNTs:TNTs-AgNP template controls and significantly enhances the product formation of PNTP from PATP in the presence of an electric field with and without UV irradiation. The electric field enabled faster and more efficient product formation of PNTP from PATP in comparison to PNTs-AgNPs or TNTs-AgNPs alone due charge transfer between the semiconducting materials and the AgNPs. Using PNTs:TNTs-AgNPs as catalysts under an

electric field, PNTP was produced from PATP in a single step process with only 10 minutes UV irradiation in comparison to 45 minutes when using PNTs-AgNPs alone. Our results demonstrate that combining semiconductors rationally offers advantages for photo- or electric field-driven catalysis.

AUTHOR INFORMATION

Corresponding Authors
*E-mail: james.rice@ucd.ie.
*E-mail: brian.rodriguez@ucd.ie.

Author Contributions S.A., A.F., B.J.R., and J.H.R. designed the experiments and developed the experimental setup. S.A. carried out sample preparation and Raman, FTIR, optical images, and SEM measurements. S.A. and A.F. carried out UV−vis experiments. All the authors analyzed the data, discussed the results, and wrote and reviewed the manuscript.

Notes The authors declare no competing financial interest.

ACKNOWLEDGMENTS

This research was funded by Science Foundation Ireland (18/TIDA/6139, 12/IP/1556, 07/IN1/B931, and SFI/17/CDA/4637). The authors acknowledge Ian Reid for assistance with SEM and Gareth Redmond for access to the UV−vis spectrometer. The authors also acknowledge Sebastian Tadeusz Barwich for assistance with IV measurements and Kevin McCarthy for 3D printing the mask used.

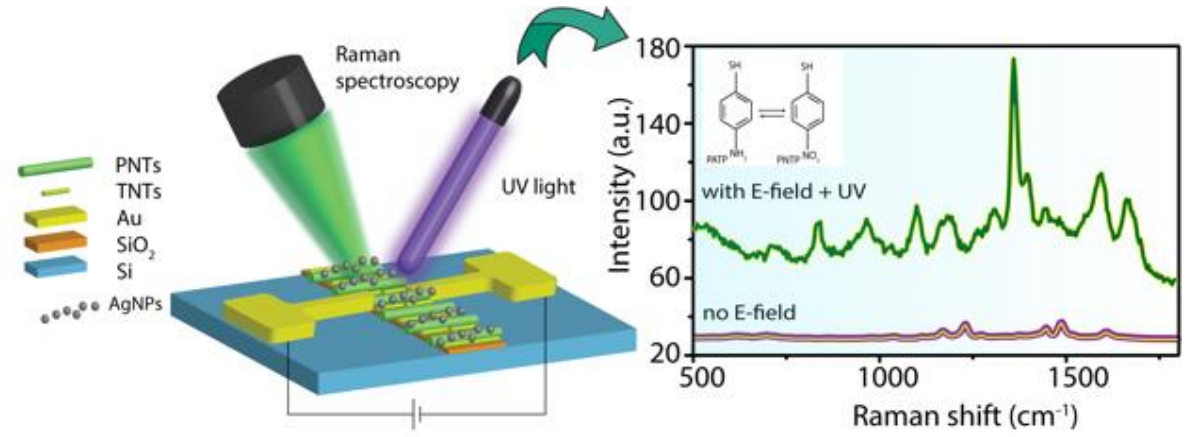

References

(1) Michaels, A. M.; Nirmal, M.; Brus, L. E. Surface Enhanced Raman Spectroscopy of Individual Rhodamine 6G Molecules on Large Ag Nanocrystals. *J. Am. Chem. Soc.* **1999**, *121* (43), 9932–9939. https://doi.org/10.1021/ja992128q.

(2) Thacker, V. V; Herrmann, L. O.; Sigle, D. O.; Zhang, T.; Liedl, T.; Baumberg, J. J.; Keyser, U. F. DNA Origami Based Assembly of Gold Nanoparticle Dimers for Surface-Enhanced Raman Scattering. *Nat. Commun.* **2014**, *5*, 3448. https://doi.org/10.1038/ncomms4448.

(3) Madzharova, F.; Heiner, Z.; Guhlke, M.; Kneipp, J. Surface-Enhanced Hyper-Raman Spectra of Adenine, Guanine, Cytosine, Thymine, and Uracil. *J. Phys. Chem. C* **2016**, *120* (28), 15415–15423. https://doi.org/10.1021/acs.jpcc.6b02753.

(4) Fularz, A.; Almohammed, S.; Rice, J. H. Oxygen Incorporation-Induced SERS Enhancement in Silver Nanoparticle-Decorated ZnO Nanowires. *ACS Appl. Nano Mater.* **2020,** (2), 1666–1673. https://doi.org/10.1021/acsanm.9b02395.

(5) Wang, J.; Ando, R. A.; Camargo, P. H. C. Controlling the Selectivity of the Surface Plasmon Resonance Mediated Oxidation of P-Aminothiophenol on Au Nanoparticles by Charge Transfer from UV-Excited TiO_2. *Angew. Chemie - Int. Ed.* **2015**, *54* (23), 6909–6912. https://doi.org/10.1002/anie.201502077.

(6) Zhang, Z.; Xu, P.; Yang, X.; Liang, W.; Sun, M. Surface Plasmon-Driven Photocatalysis in Ambient, Aqueous and High-Vacuum Monitored by SERS and TERS. *J. Photochem. Photobiol. C Photochem. Rev.* **2015**, *27* (April), 100–112. https://doi.org/10.1016/j.jphotochemrev.2016.04.001.

(7) Park, W.-H.; Kim, Z. H. Charge Transfer Enhancement in the SERS of a Single Molecule. *Nano Lett.* **2010**, *10* (10), 4040–4048. https://doi.org/10.1021/nl102026p.

(8) Zhou, N.; López-Puente, V.; Wang, Q.; Polavarapu, L.; Pastoriza-Santos, I.; Xu, Q. H. Plasmon-Enhanced Light Harvesting: Applications in Enhanced Photocatalysis, Photodynamic Therapy and Photovoltaics. *RSC Adv.* **2015**, *5* (37), 29076–29097. https://doi.org/10.1039/c5ra01819f.

(9) Ma, L.; Huang, Y.; Hou, M.; Xie, Z.; Zhang, Z. Ag Nanorods Coated with Ultrathin TiO_2 Shells as Stable and Recyclable SERS Substrates. *Sci. Rep.* **2015**, *5*, 15442. https://doi.org/10.1038/srep15442.

(10) Ben-Jaber, S.; Peveler, W. J.; Quesada-Cabrera, R.; Cortés, E.; Sotelo-Vazquez, C.; Abdul-Karim, N.; Maier, S. A.; Parkin, I. P. Photo-Induced Enhanced Raman Spectroscopy for Universal Ultra-Trace Detection of Explosives, Pollutants and Biomolecules. *Nat. Commun.* **2016**, *7* (May), 12189. https://doi.org/10.1038/ncomms12189.

(11) Yilmaz, M.; Babur, E.; Ozdemir, M.; Gieseking, R. L.; Dede, Y.; Tamer, U.; Schatz, G. C.; Facchetti, A.; Usta, H.; Demirel, G. Nanostructured Organic Semiconductor Films for Molecular Detection with Surface-Enhanced Raman Spectroscopy. *Nat. Mater.* **2017**, *16* (9), 918–924. https://doi.org/10.1038/nmat4957.

(12) Roller, E.; Schreiber, R.; Liedl, T.; Feldmann, J. Plasmonic DNA-Origami Nanoantennas for Surface-Enhanced Raman Spectroscopy. *Nano Lett.* **2014**, 14 (5), 2914-2919. https://doi.org/10.1021/nl5009635.

(13) Lee, K.; Irudayaraj, J. Periodic and Dynamic 3-D Gold Nanoparticle−DNA Network Structures for Surface-Enhanced Raman Spectroscopy-Based Quantification. *J. Phys. Chem. C* **2009**, *113* (15), 5980–5983. https://doi.org/10.1021/jp809949v.

(14) Huang, J. A.; Zhao, Y. Q.; Zhang, X. J.; He, L. F.; Wong, T. L.; Chui, Y. S.; Zhang, W. J.;

Lee, S. T. Ordered Ag/Si Nanowires Array: Wide-Range Surface-Enhanced Raman Spectroscopy for Reproducible Biomolecule Detection. *Nano Lett.* **2013**, *13* (11), 5039–5045. https://doi.org/10.1021/nl401920u.

(15) Nuraeva, A.; Vasilev, S.; Vasileva, D.; Zelenovskiy, P.; Chezganov, D.; Esin, A.; Kopyl, S.; Romanyuk, K.; Shur, V. Y.; Kholkin, A. L. Evaporation-Driven Crystallization of Diphenylalanine Microtubes for Microelectronic Applications. *Cryst. Growth Des.* **2016**, *16* (3), 1472–1479. https://doi.org/10.1021/acs.cgd.5b01604.

(16) Adler- Abramovich, L.; Reches, M.; Sedman, V. L.; Allen, S.; Tendler, S. J. B.; Gazit, E. Thermal and Chemical Stability of Diphenylalanine Peptide Nanotubes: Implications for Nanotechnological Applications. *Langmuir* **2006**, *22* (20), 1313. https://doi.org/10.1021/la052409d.

(17) Kim, J.; Han, T. H.; Kim, Y. Il; Park, J. S.; Choi, J.; Churchill, D. G.; Kim, S. O.; Ihee, H. Role of Water in Directing Diphenylalanine Assembly into Nanotubes and Nanowires. *Adv. Mater.* **2010**, *22* (5), 583–587. https://doi.org/10.1002/adma.200901973.

(18) Chen, J.; Qin, S.; Wu, X.; Chu, A. P. K. Morphology and Pattern Control of Diphenylalanine Self-Assembly via Evaporative Dewetting. *ACS Nano* **2016**, *10* (1), 832–838. https://doi.org/10.1021/acsnano.5b05936.

(19) Bdikin, I.; Bystrov, V.; Kopyl, S.; Lopes, R. P. G.; Delgadillo, I.; Gracio, J.; Mishina, E.; Sigov, A.; Kholkin, A. L. Evidence of Ferroelectricity and Phase Transition in Pressed Diphenylalanine Peptide Nanotubes. *Appl. Phys. Lett.* **2012**, *100* (4), 043702. https://doi.org/10.1063/1.3676417.

(20) Takahashi, R.; Wang, H.; Lewis, J. P. Electronic Structures and Conductivity in Peptide Nanotubes. *J. Phys. Chem. B* **2007**, *111* (30), 9093–9098. https://doi.org/10.1021/jp0708446.

(21) Santhanamoorthi, N.; Kolandaivel, P.; Adler-Abramovich, L.; Gazit, E.; Filipek, S.; Viswanathan, S.; Strzelczyk, A.; Renugopalakrishnan, V. Diphenylalanine Peptide Nanotube: Charge Transport, Band Gap and Its Relevance to Potential Biomedical Applications. *Adv. Mater. Lett.* **2011**, *2* (2), 100–105. https://doi.org/10.5185/amlett.2010.12223.

(22) Fan, Z.; Sun, L.; Huang, Y.; Wang, Y.; Zhang, M. Bioinspired Fluorescent Dipeptide Nanoparticles for Targeted Cancer Cell Imaging and Real-Time Monitoring of Drug Release. *Nat. Nanotechnol.* **2016**, *11* (January), 388–394. https://doi.org/10.1038/nnano.2015.312.

(23) Kasotakis, E.; Mossou, E.; Adler-Abramovich, L.; Mitchell, E. P.; Forsyth, V. T.; Gazit, E.; Mitraki, A. Design of Metal-Binding Sites onto Self-Assembled Peptide Fibrils. *Biopolymers* **2009**, *92* (3), 164–172. https://doi.org/10.1002/bip.21163.

(24) Erdogan, H.; Sakalak, H.; Yavuz, M. S.; Demirel, G. Laser-Triggered Degelation Control of Gold Nanoparticle Embedded Peptide Organogels. *Langmuir* **2013**, *29* (23), 6975–6982. https://doi.org/10.1021/la401300u.

(25) George, J.; George Thomas, K. Surface Plasmon Coupled Circular Dichroism of Au Nanoparticles on Peptide Nanotubes. *J. Am. Chem. Soc.* **2010**, *132* (8), 2502–2503. https://doi.org/10.1021/ja908574j.

(26) Reches, M.; Gazit, E. Casting Metal Nanowires within Discrete Self-Assembled Peptide Nanotubes. *Science* **2003**, *300* (5619), 625–627. https://doi.org/10.1126/science.1082387.

(27) Ryu, J.; Lim, S. Y.; Park, C. B. Photoluminescent Peptide Nanotubes. *Adv. Mater.* **2009**, *21* (16), 1577–1581. https://doi.org/10.1002/adma.200802700.

(28) Souza, M. I.; Jaques, Y. M.; De Andrade, G. P.; Ribeiro, A. O.; Da Silva, E. R.; Fileti, E. E.; Ávilla, É. D. S.; Pinheiro, M. V. B.; Krambrock, K.; Alves, W. a. Structural and Photophysical Properties of Peptide Micro/Nanotubes Functionalized with Hypericin. *J. Phys. Chem. B* **2013**, *117*, 2605–2614. https://doi.org/10.1021/jp3113655.

(29) Almohammed, S.; Zhang, F.; Rodriguez, B. J.; Rice, J. H. Electric Field-Induced Chemical SERS Enhancement from Aligned Peptide Nanotube–Graphene Oxide Templates for Universal Trace Detection of Biomolecules. *J. Phys. Chem. Lett.* **2019**, 10, 1878-1887. https://doi.org/10.1021/acs.jpclett.9b00436.

(30) Ivanov, M. S.; Khomchenko, V. A.; Salimian, M.; Nikitin, T.; Kopyl, S.; Buryakov, A. M.; Mishina, E. D.; Salehli, F.; Marques, P. A. A. P.; Goncalves, G.; et al. Self-Assembled Diphenylalanine Peptide Microtubes Covered by Reduced Graphene Oxide/Spiky Nickel Nanocomposite: An Integrated Nanobiomaterial for Multifunctional Applications. *Mater. Des.* **2018**, *142*, 149–157. https://doi.org/10.1016/j.matdes.2018.01.018.

(31) Castillo, J.; Tanzi, S.; Dimaki, M.; Svendsen, W. Manipulation of Self-Assembly Amyloid Peptide Nanotubes by Dielectrophoresis. *Electrophoresis* **2008**, *29* (24), 5026–5032. https://doi.org/10.1002/elps.200800260.

(32) Almohammed, S.; Zhang, F.; Rodriguez, B. J.; Rice, J. H. Photo-Induced Surface-Enhanced Raman Spectroscopy from a Diphenylalanine Peptide Nanotube-Metal Nanoparticle Template. *Sci. Rep.* **2018**, *8* (1), 3880. https://doi.org/10.1038/s41598-018-22269-x.

(33) Wang, W.; Anderson, C. F.; Wang, Z.; Wu, W.; Cui, H.; Liu, C.J. Peptide-Templated Noble Metal Catalysts: Syntheses and Applications. *Chem. Sci.* **2017**, *8* (5), 3310–3324. https://doi.org/10.1039/C7SC00069C.

(34) Wang, C. F.; O'Callahan, B. T.; Kurouski, D.; Krayev, A.; El-Khoury, P. Z. The Prevalence of Anions at Plasmonic Nanojunctions: A Closer Look at p-Nitrothiophenol. *J. Phys. Chem. Lett.* **2020**, *11* (10), 3809–3814. https://doi.org/10.1021/acs.jpclett.0c01006.

(35) Andrade-Filho, T.; Ferreira, F. F.; Alves, W. A.; Rocha, A. R. The Effects of Water Molecules on the Electronic and Structural Properties of Peptide Nanotubes. *Phys. Chem. Chem. Phys.* **2013**, *15* (20), 7555. https://doi.org/10.1039/c3cp43952f.

(36) Esin, A.; Baturin, I.; Nikitin, T.; Vasilev, S.; Salehli, F.; Shur, V. Y.; Kholkin, A. L. Pyroelectric Effect and Polarization Instability in Self-Assembled Diphenylalanine Microtubes. *Appl. Phys. Lett.* **2016**, *109* (14), 1–5. https://doi.org/10.1063/1.4962652.

(37) Almohammed, S.; Tade Barwich, S.; Mitchell, A. K.; Rodriguez, B. J.; Rice, J. H. Enhanced Photocatalysis and Biomolecular Sensing with Field-Activated Nanotube-Nanoparticle Templates. *Nat. Commun.* **2019**, *10* (1), 2496. https://doi.org/10.1038/s41467-019-10393-9.

(38) Choi, H.; Shin, J.; Shin, C. Impact of Source/Drain Metal Work Function on the Electrical Characteristics of Anatase TiO_2-Based Thin Film Transistors. *ECS J. Solid State Sci. Technol.* **2017**, *6* (7), P379–P382. https://doi.org/10.1149/2.0121707jss.

(39) Kashiwaya, S.; Morasch, J.; Streibel, V.; Toupance, T.; Jaegermann, W.; Klein, A. The Work Function of TiO_2. *Surfaces* **2018**, *1* (1), 73–89. https://doi.org/10.3390/surfaces1010007.

(40) Yang, Q.; Hu, M.; Guo, J.; Ge, Z.; Feng, J. Synthesis and Enhanced Photocatalytic Performance of Ag/AgCl/TiO_2 Nanocomposites Prepared by Ion Exchange Method. *J. Mater.* **2018**, *4* (4), 402–411. https://doi.org/10.1016/j.jmat.2018.06.002.

(41) Tonomura, O.; Sekiguchi, T.; Inada, N.; Hamada, T.; Miki, H.; Torii, K. Band Engineering

of Ru/Rutile-TiO_2/Ru Capacitors by Doping Cobalt to Suppress Leakage Current. *J. Electrochem. Soc.* **2012**, *159* (1), 1–5. https://doi.org/10.1149/2.040201jes.

(42) Guo, L. Q.; Hu, Y. W.; Yu, B.; Davis, E.; Irvin, R.; Yan, X. G.; Li, D. Y. Incorporating TiO_2 nanotubes with a Peptide of D-Amino K122-4 (D) for Enhanced Mechanical and Photocatalytic Properties. *Sci. Rep.* **2016**, *6* (February), 1–10. https://doi.org/10.1038/srep22247.

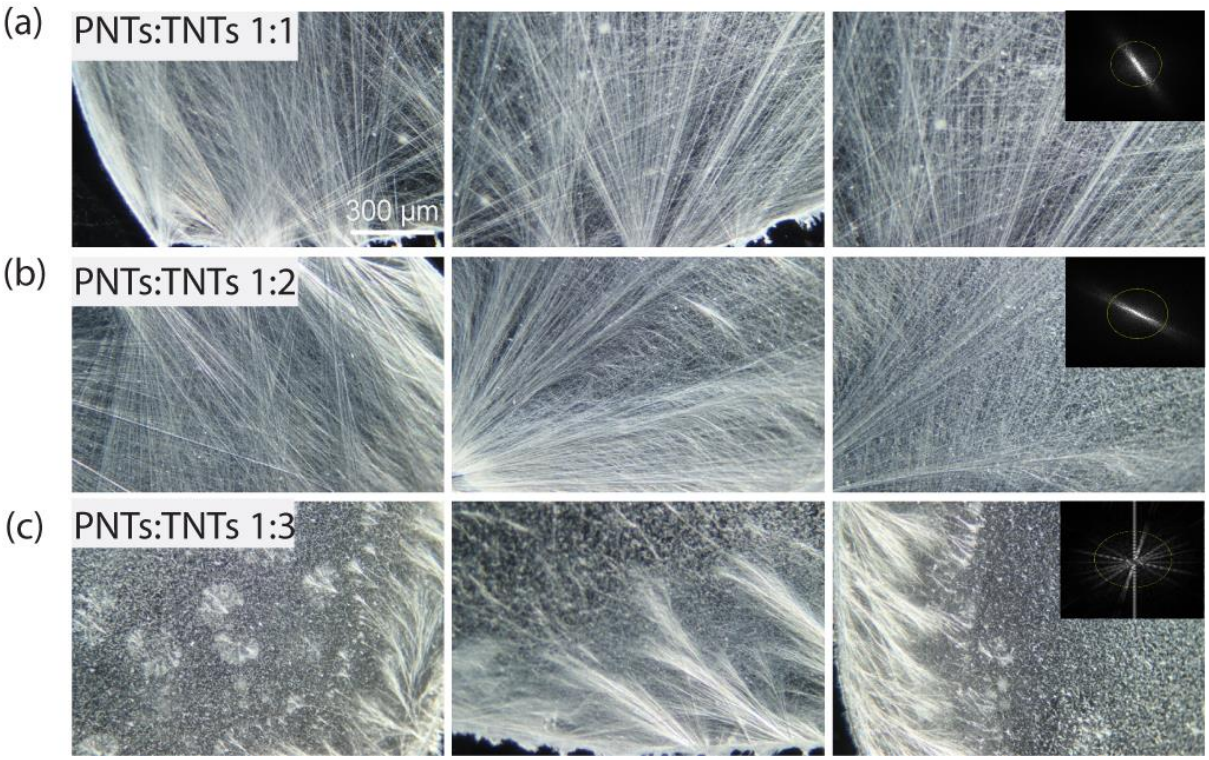

Figure S1. (a-c) Optical microscopy images of PNTs:TNTs prepared with ratios of 1:1, 1:2, and 1:3, respectively. Each image is from a different sample. The degree of alignment was determined following a previously reported procedure.[1] The alignment was quantified as the mean and standard deviation of the full width at half maximum (FWHM) of the radial summation of the fast Fourier transforms (FFTs) of the three optical microscopy images shown to be 17 ± 2 °, 19 ± 3 °, and 68 ± 5 ° for (a-c), respectively. The yellow circles in the FFT images are circular projection output by which a graphical of the FFT frequency distribution can be generated and conducting a radial summation of the pixel intensities. The insets in the last column are FFT images of the optical images in the same column. The PNTs aligned according to the wettability difference (the samples were rotated for imaging) for ratios of 1:1 and 1:2; however, alignment was reduced for 1:3.

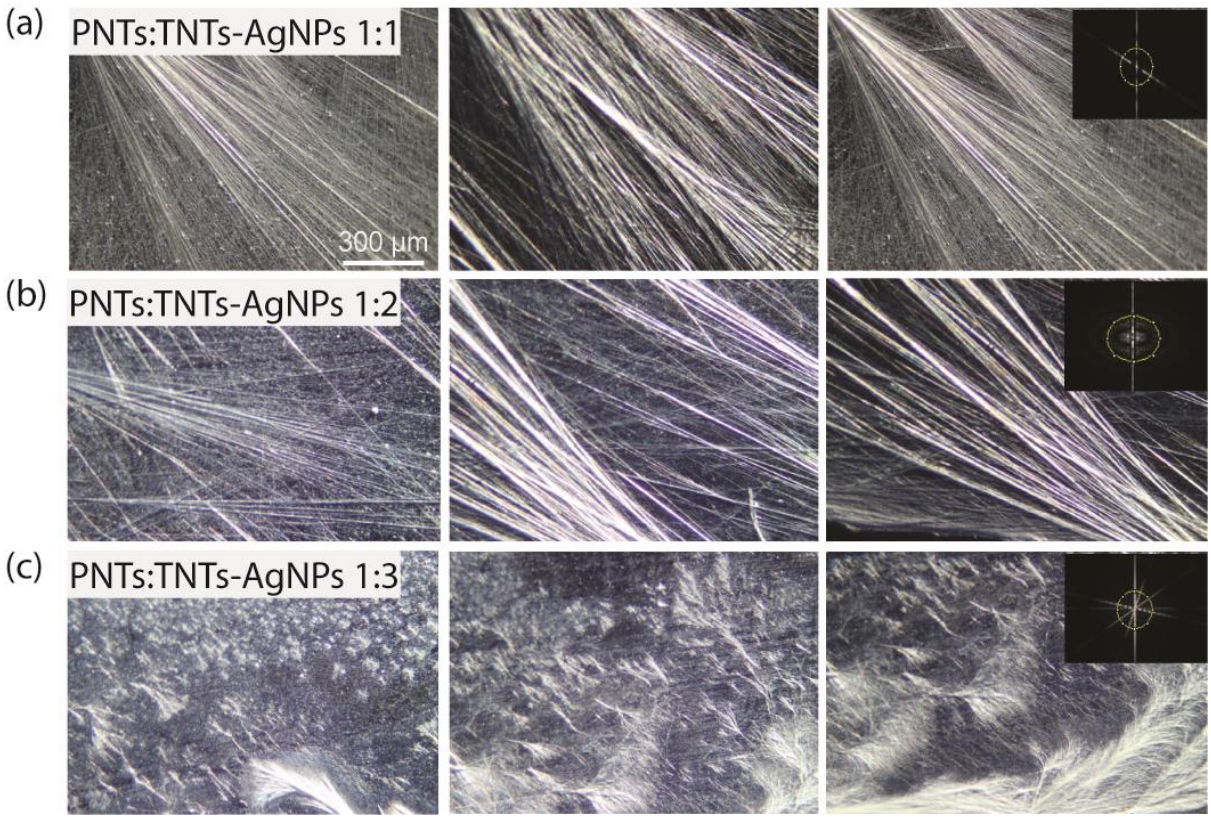

Figure S2. (a-c) Optical microscopy images of PNTs:TNTs-AgNP templates prepared at different PNTs:TNTs ratios. Each image is from a different sample. The degree of alignment was determined following a previously reported procedure.[1] The alignment was quantified as the mean and standard deviation of the FWHM of the radial summation of the FFTs of the three optical microscopy images shown to be 15 ± 3 °, 18 ± 4 °, and 67 ± 5 ° for (a-c), respectively. The insets in the last column are FFT images of the optical images in the same column. The yellow circular in the FFT images are circular projection output by which a graphical of the FFT frequency distribution can be generated and conducting a radial summation of the pixel intensities.

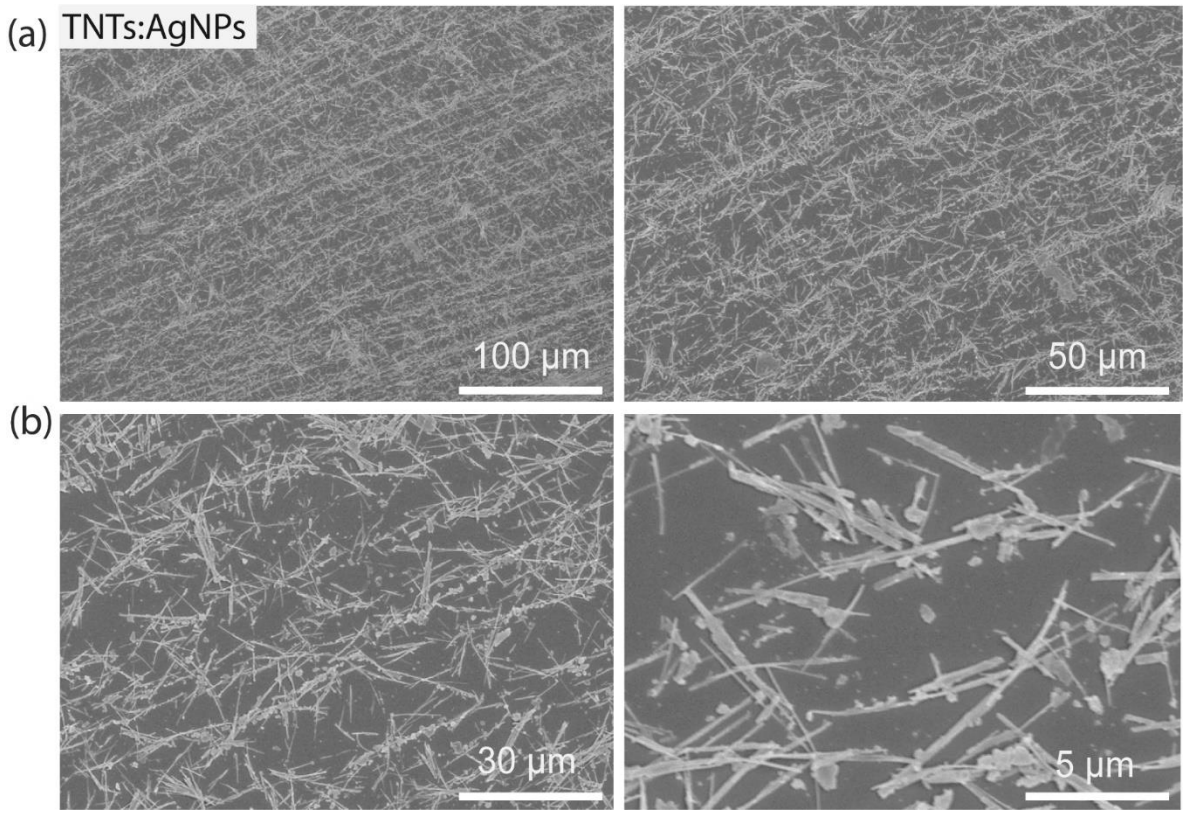

Figure S3. (a,b) SEM images of TNTs:AgNPs at a ratio of 1:1.

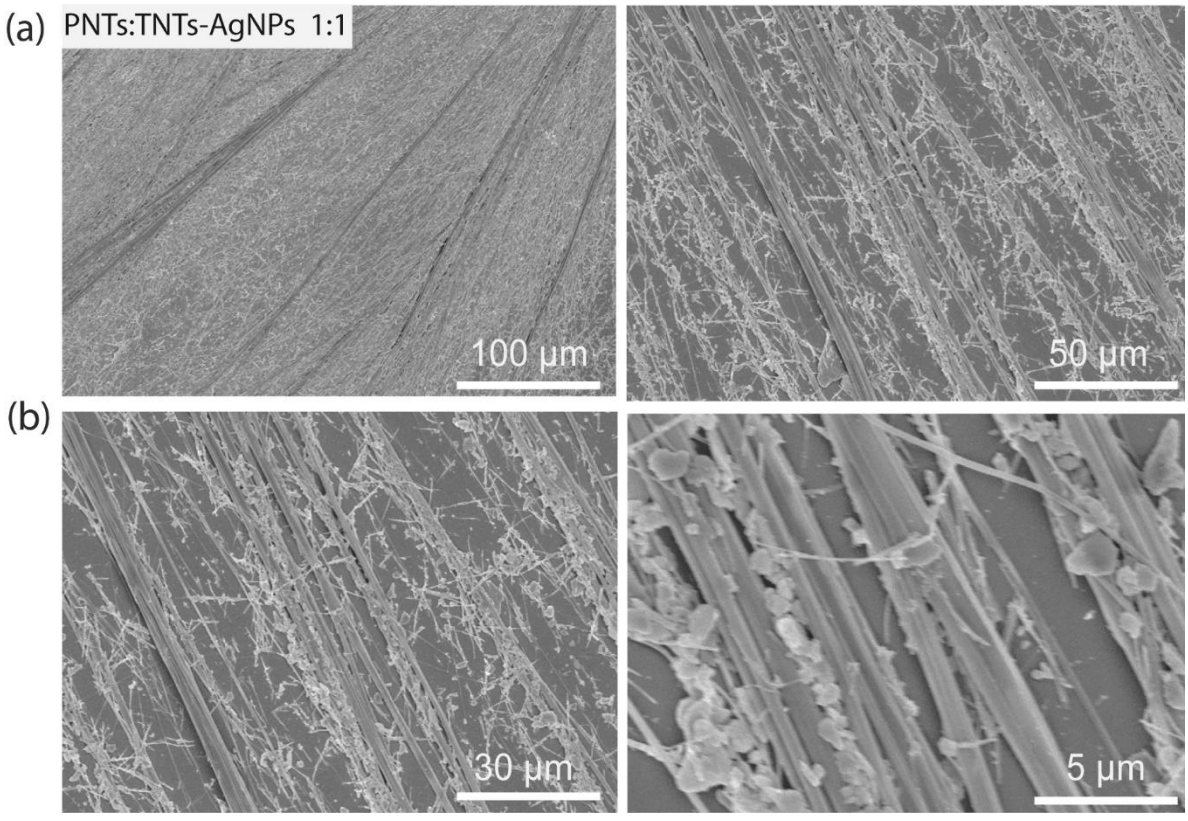

Figure S4. (a,b) SEM images of PNTs:TNTs-AgNP templates at a 1:1 PNTs:TNTs ratio.

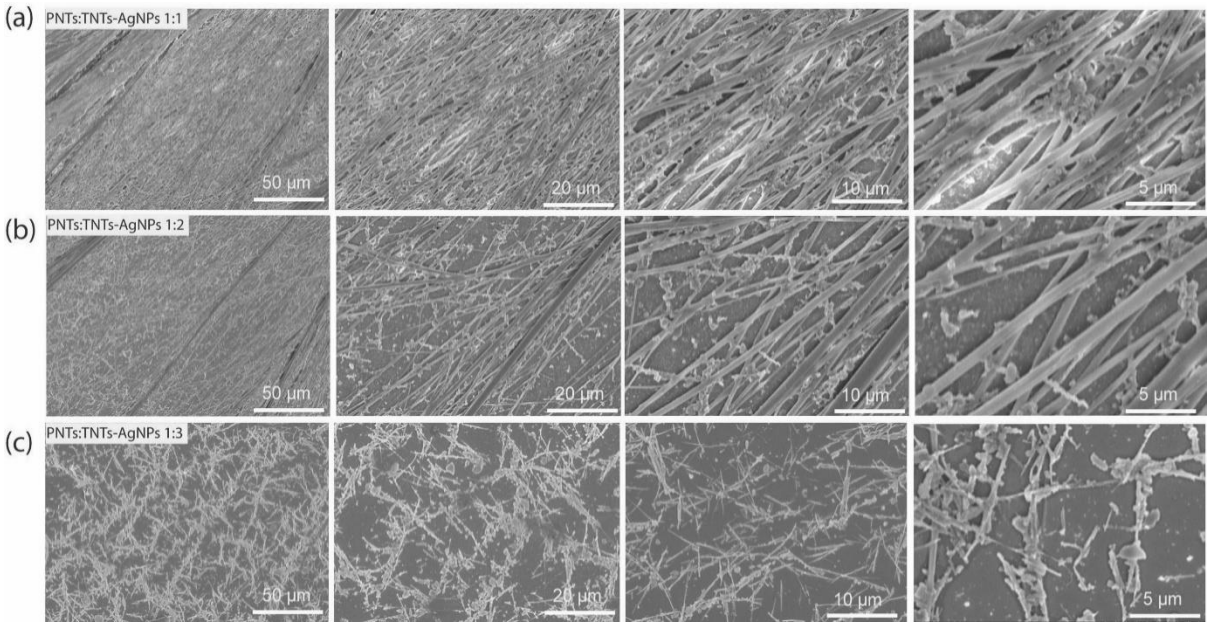

Figure S5. (a–c) SEM images of PNTs:TNTs-AgNP templates prepared at PNTs:TNTs ratios of 1:1, 1:2, and 1:3, respectively.

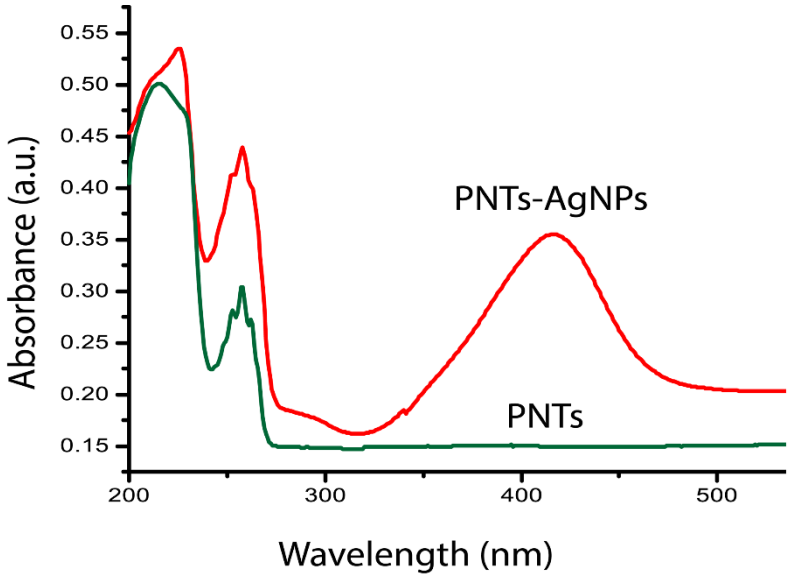

Figure S6. Absorption measurements of PNTs and PNTs-AgNPs.

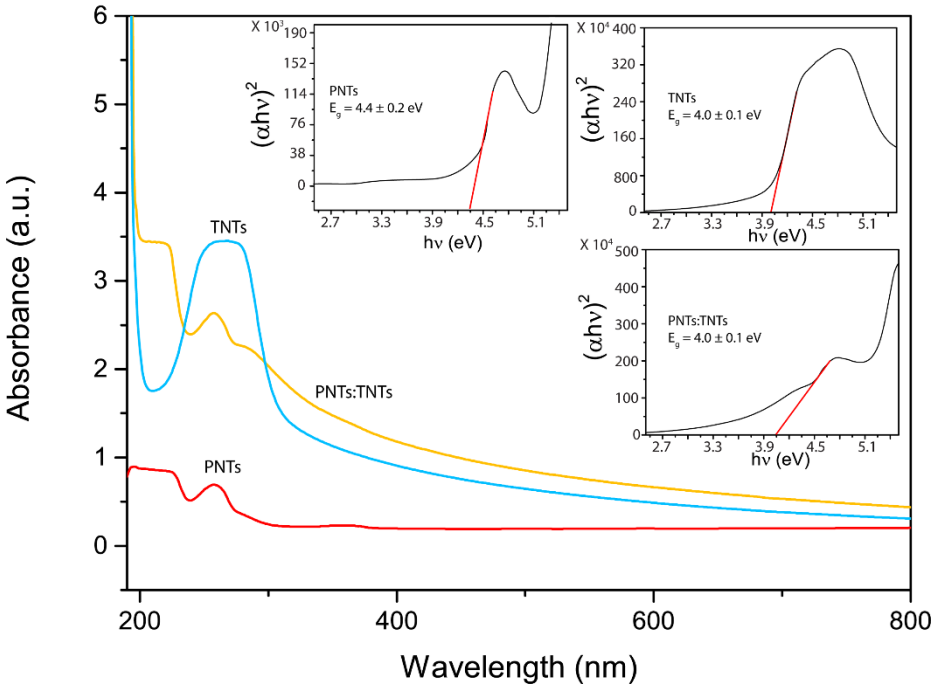

Figure S7. UV-vis measurements of PNTs with and without TNTs.

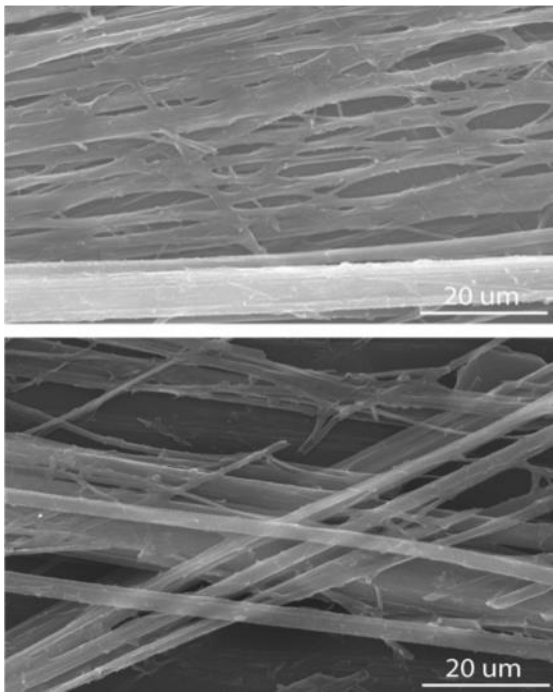

Figure S8. SEM images of PNTs:TNTs (1:1) after adding the probe molecule PATP.

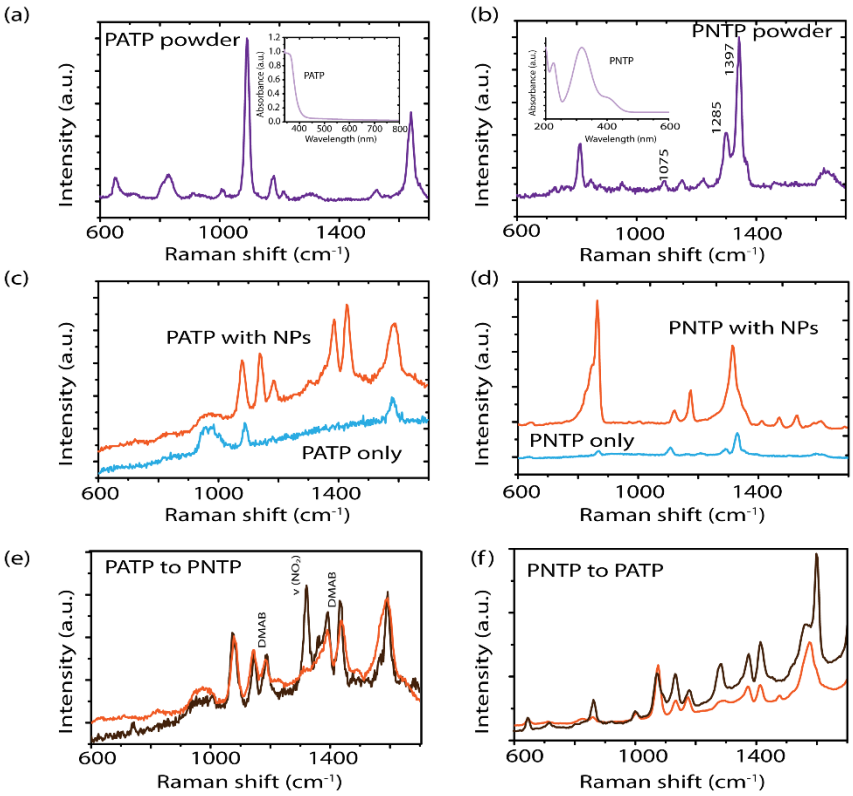

Figure S9. (a,b) Raman spectra of PATP and PNTP in powder form; the insets in (a) and (b) are the absorbance spectra of PATP and PNTP recorded in solution, which show that PATP possesses a band in the ultraviolet region and PNTP has absorption bands located between 200–480 nm. The Raman spectrum for PATP in powder form (a) shows peaks at 1081, 1182, 1489, and 1593 cm^{-1} that are assigned to a_1 type vibrations.[2,3–4] (c) SERS spectra of PATP on the template (with AgNPs orange spectra) versus on a Si substrate only, without metal NPs (blue spectra). The SERS spectra for PATP on the template in the presence of metal (orange spectra) is assigned to a combination of a- and b-type vibrational bands. Four of the five most intense bands (at 1142, 1390, 1433, and 1575 cm^{-1}) are attributed to b_2 modes. The band at 1082 cm^{-1} is assigned to an a_1 mode. The four non-totally symmetric b_2 modes originate from a photochemical reaction of PATP to form p,p'-dimercaptoazobenzene (DMAB)[5–7] with the b_2 vibrations of N=N at 1433 and 1390 cm^{-1} and the 1142 cm^{-1} peak assigned as a C-N vibrational mode.[5–7] In contrast, PATP without metal NPs (blue spectra) shows band associated with only vibrational modes with a_1 symmetry at 1088 and 1594 cm^{-1}, which are assigned to the Raman spectrum of PATP according to the literature.[2,3–4] It should be emphasized that no catalyst activity was observed in the absence of NPs. (d) SERS spectra of PNTP on the template with AgNPs (orange spectra) versus on a Si substrate only, without metal nanoparticles (blue spectra). The SERS spectra for PNTP on the template (with AgNPs orange spectra) has bands located at 1571, 1435, 1389, 1333, 1141, 1079, 1058, and 858 cm^{-1}.[8–11] (e) PATP on the PNTs:TNTs-AgNP template is transformed into a mixture of PNTP and DMAB with applied DC voltage and UV irradiation, characterized by the appearance of a NO_2 vibrational (v) peak at 1333 cm^{-1}. The strong bands at 1433, 1390, and 1142 cm^{-1} from DMAB and weak peak at 1333 cm^{-1} due to the NO_2 vibration of PNTP.[8–11] (f) PNTP on a PNTs:TNTs-AgNP template is transformed into PATP with applied DC voltage and UV irradiation, characterized by the disappearance of the vibrational NO_2 peak at ~ 1333 cm^{-1}, and other bands at 1058 and 858 cm^{-1}, which are associated with PNTP anions.

In Fig. S9, we show the pure-powder form of PATP and PNTP with and without NPs. The obtained DMAB spectrum is fully consistent with previously reported spectra of the same species.[8–11]

The full spectral features of the anionic species in the 800−1600 cm^{-1} range are also visible in Fig. S9. Specifically, peaks in the spectrum of the PNTP powder at 1075, 1285 and 1397 cm^{-1} are associated with the presence of trace amounts of PNTP anions.[11] Those peaks are less pronounced than those of PNTP following oxidation (the peaks associated with the PNTP anions are of lower intensity than those of the PNTP product) and therefore, the analyte becomes almost completely oxidized following the application of UV irradiation/electric field (Fig. 3).

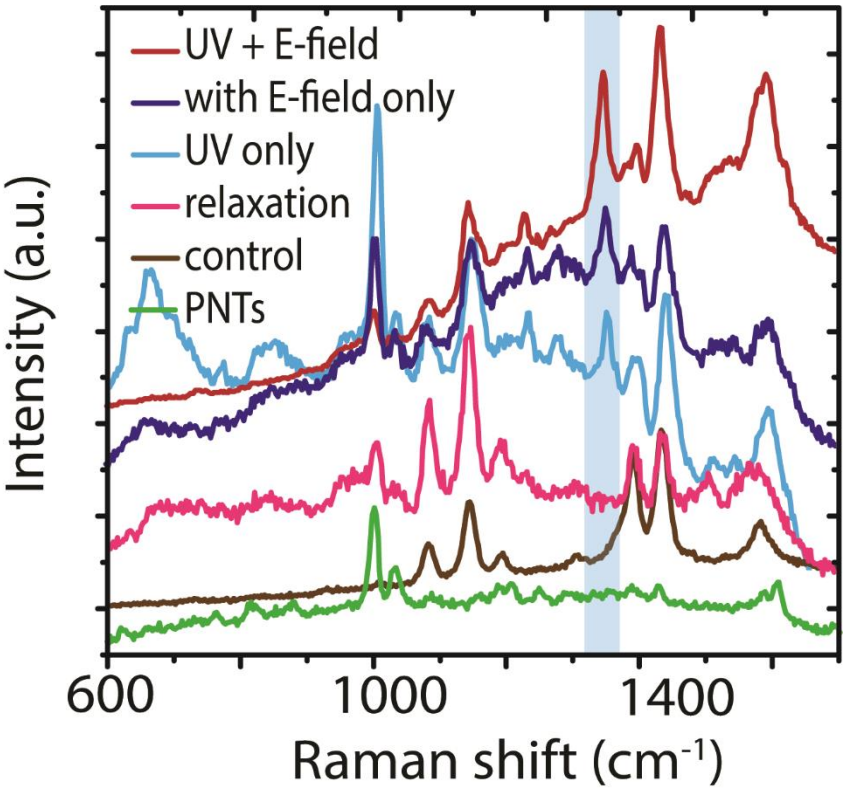

Figure S10. Representative SERS spectra of PATP on PNTs:TNTs-AgNPs templates recorded under different conditions. The 254 nm UV irradiation is super bandgap. Electric field (E-field) refers to the field generated by the application of DC voltage. Relaxation refers to SERS spectra recorded after the UV or DC voltage is removed. Control refers to the SERS spectra before DC voltage or UV is applied. The blue shading indicates the position of the 1333 cm^{-1} Raman band arising from PNTP.

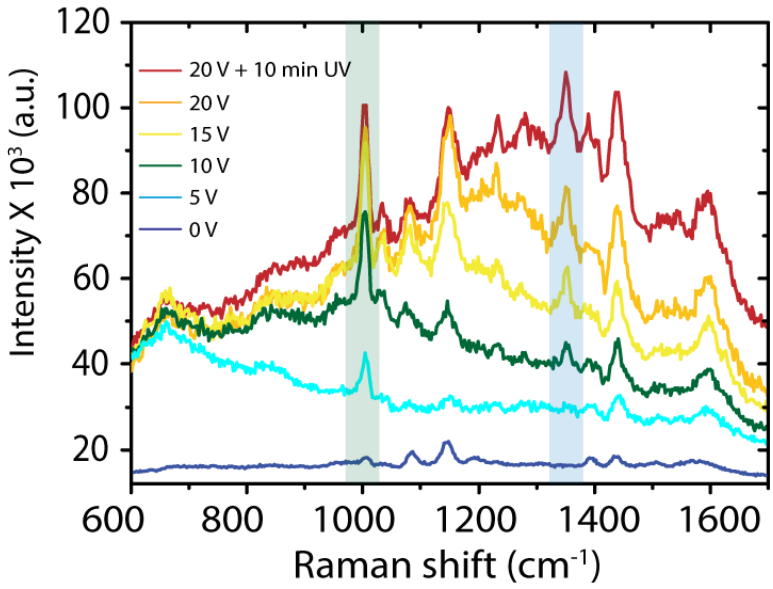

Figure S11. SERS spectra of PATP on PNTs-AgNPs (in the absence of TNTs) with applied DC voltage. The blue shading marks the position of the 1333 cm^{-1} Raman band arising from PNTP, whereas the green shading refers to the breathing mode for PNTs located at ~ 1000 cm^{-1}.

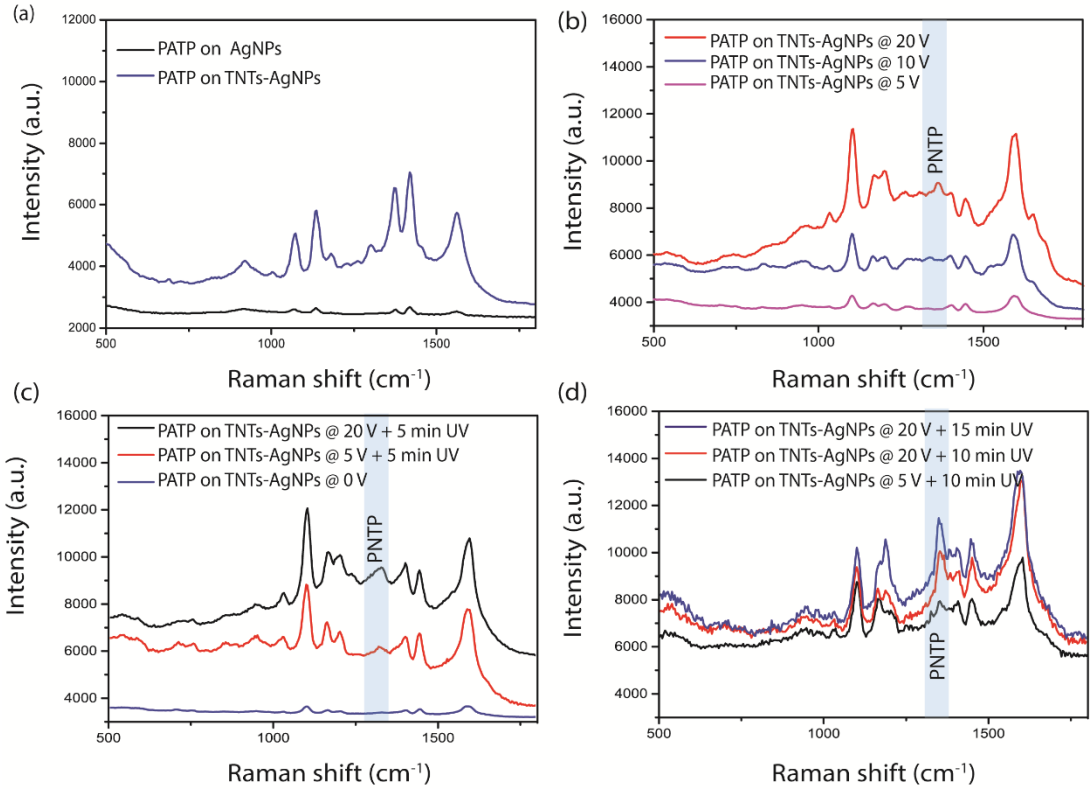

Figure S12. (a) SERS spectra of PATP on TNTs-AgNPs (in the absence of PNTs) with applied DC voltage and (b, c) with both DC voltage and UV irradiation. The 254 nm UV irradiation is super bandgap. The blue shading marks the position of the 1333 cm^{-1} Raman band arising from PNTP.

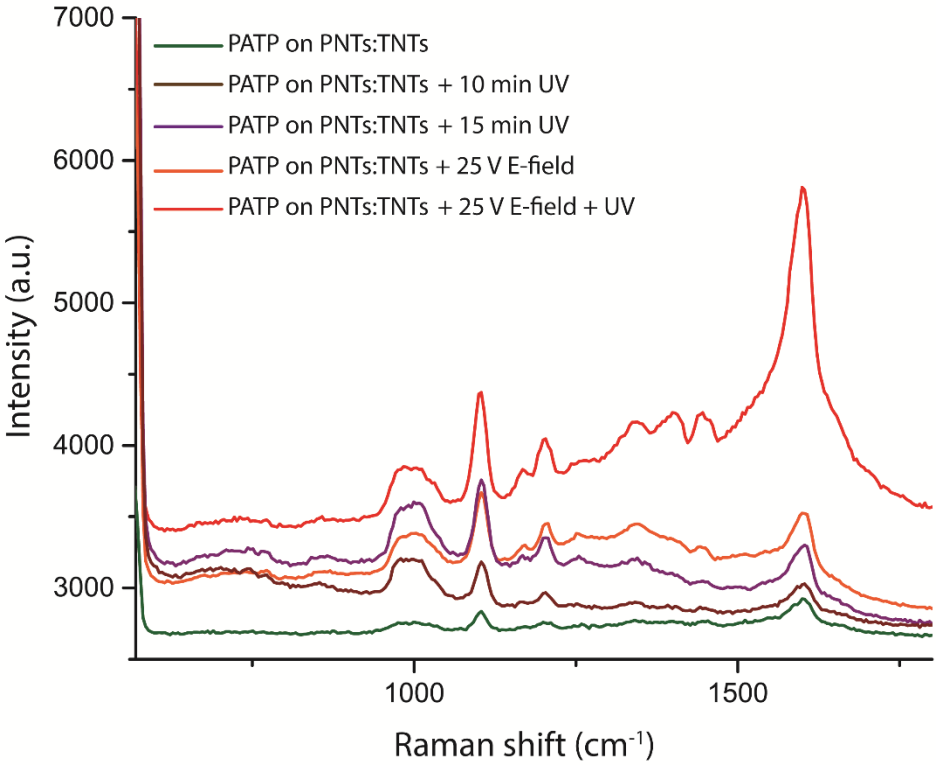

Figure S13. (a) SERS measurement of PNTs:TNTs and PATP with and without electric field (generated by application of DC voltage) and UV irradiation in the absence of metal NPs.

The SERS spectrum recorded for PATP on the PNTs:TNTs prior to applying an electric field or UV irradiation shows only vibrational modes with a_1 symmetry, such as bands located at 1088 and 1594 cm^{-1}, which are assigned to the Raman spectrum of the PATP in the literature.[12] Through the application of an electric field (with and without UV), the Raman spectral features started to change with b_2 mode bands (1433, 1390, 1142, and 1076 cm^{-1}) appearing. According to the literature, the PATP Raman b_2 modes can be seen due to photochemical reaction of PATP to form p,p'-dimercaptoazobenzene (DMAB).[12] The ability to observe these bands in the absence of metal NPs in this work could be due to super bandgap UV excitation of the PNTs (4.8 eV UV excitation is greater than the bandgap of PNTs, E_g ~ 4.6 eV). Also, the application of electric field results in the piezoelectric activation of the PNTs possibly providing piezoelectric charge that can be involved in charge transfer processes with the probe molecules.[13] Charge-transfer between PNTs and TNTs are also possible as the work function of the PNTs is around ~6.2 eV while the work function of TNTs is 4.4 eV.[12] Thus, the difference between the Fermi level of PNTs and TNTs is ~1.8 eV, which is less than the Raman laser excitation (532 nm; 2.3 eV). Therefore, it is possible that the energy of the Raman excitation laser can facilitate the transfer of charge from PNTs to TNTs.[12]

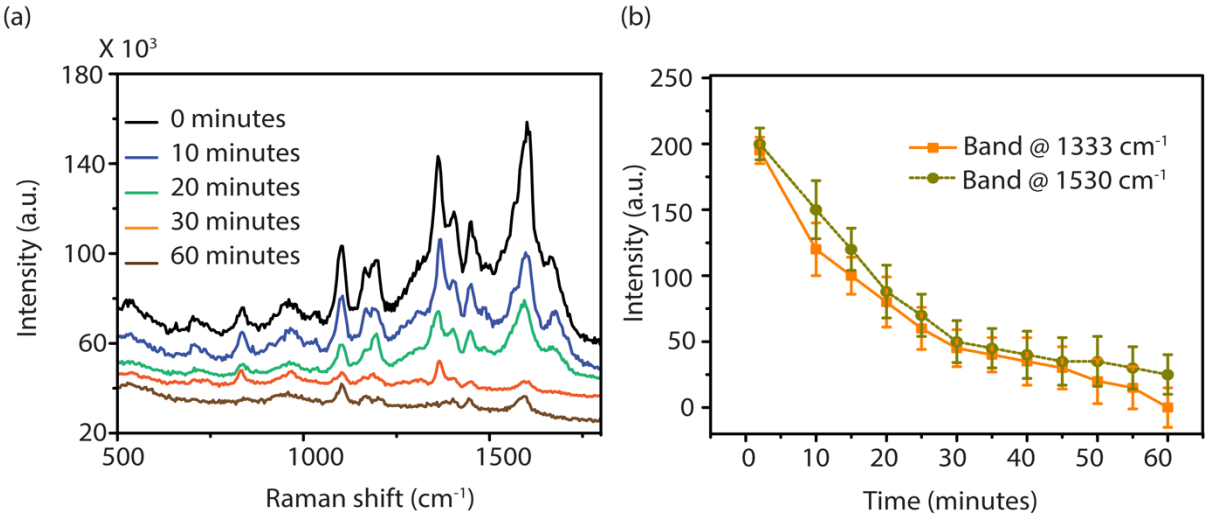

Figure S14. (a) SERS measurements of PATP on the template after removing electric field and UV irradiation, showing relaxation over time of both SERS intensity and the product formation. (b) Plot of SERS intensity of the band at 1530 cm^{-1} for PATP and the product formation band at 1333 cm^{-1} as a function of time. Data was collected from 6 locations each of 3 samples and averaged.

The data for product formation is shown in Fig. 3. The product formation was determined as the relative intensity of the band located at 1333 cm^{-1}, which is a strong indication of the transformation from PATP to PNTP (Fig. 3(c)). The enhancement factor was estimated as I_{SERS}/I_{Raman} and assuming the number of molecules is the same (the same drop size was used in all cases). The peak to peak intensity for the band at 1333 cm^{-1} (product) at 30 minutes relaxation time is ~ 5 versus ~ 45 at 0 minutes. Thus, we can estimate the enhancement of the product formation to be ~ 9-fold; the uncertainty reported in Figs. 3 and S14(b) reflects measurements recorded from 6 locations each on 3 samples. The signal corresponding to PATP to PNTP transformation relaxes reversibly after approximately 30–60 minutes depending on the DC voltage applied (Fig. S14). When the UV irradiation is off and no voltage is applied, there is no reaction and only the peaks of PATP can be observed in SERS. When UV irradiation is on and 20 V is applied, electrons transfer from PNTs:TNTs to AgNPs and convert PATP directly to PNTP. When UV irradiation and DC voltage are removed, hot electrons transfer to the PNTP, driving its reduction to DMAB.[5–7] Thus, the catalytic reactions can be realized with the assistance of such a semiconductor-based hybrid system.

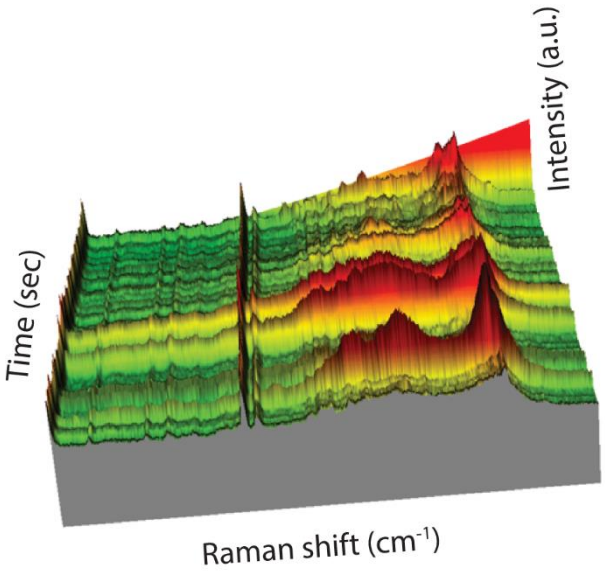

Figure S15. SERS spectra in the range of 180–1800 cm^{-1} from PNTs:TNTs-AgNPs (no probe molecules) over the course of 100 seconds in the presence of electric field (50 V/mm) and following 15 minutes of UV irradiation.

Bands in Fig. S15 at 180–280 cm^{-1} are due to lattice vibrations and those at 280–1800 cm^{-1} are associated with vibrations of peptide functional groups. Bands located at 1002 and 1032 cm^{-1} are attributed to the vibration of phenyl rings.[14,15] Bands at 1250–1686 cm^{-1} (attributed to the amide III vibrations and the amide I band) and 1800 cm^{-1} are strongly influenced by the electric field and UV irradiation and are attributed to water loss in the nanochannels of the PNTs.[16] This becomes apparent for DC voltage > 30 V and UV irradiation of ~ 15 min. The bands located at 1002 and 1003 cm^{-1}, are not affected by heat generated from the application of DC voltage, as they are considered to be the strongest spectral lines for peptide-based materials.[14,15]

References

(1) Almohammed, S.; Oladapo, S. O.; Ryan, K.; Kholkin, A. L.; Rice, J. H.; Rodriguez, B. J. Wettability Gradient-Induced Alignment of Peptide Nanotubes as Templates for Biosensing Applications. *RSC Adv.* **2016**, *6* (48), 41809–41815. https://doi.org/10.1039/C6RA05732B.

(2) Kim, K.; Kim, K. L.; Lee, H. B.; Shin, K. S. Similarity and Dissimilarity in Surface-Enhanced Raman Scattering of Dimercaptohydrazobenzene on Ag. *J. Phys. Chem. C* **2012**, *116* (21), 11635–11642. https://doi.org/10.1021/jp303378p

(3) Sun, M.; Xu, H. Direct Visualization of the Chemical Mechanism in SERRS of 4-Aminothiophenol/Metal Complexes and Metal/4-Aminothiophenol/Metal Junctions. *ChemPhysChem* **2009**, *10* (2), 392–399. https://doi.org/10.1002/cphc.200800596.

(4) Zhang, Z.; Xu, P.; Yang, X.; Liang, W.; Sun, M. Surface Plasmon-Driven Photocatalysis in Ambient, Aqueous and High-Vacuum Monitored by SERS and TERS. *J. Photochem. Photobiol. C Photochem. Rev.* **2016**, *27*, 100–112. https://doi.org/10.1016/j.jphotochemrev.2016.04.001.

(5) Wang, H. Mechanistic Understanding of Surface Plasmon Assisted Catalysis on a Single Particle: Cyclic Redox of 4-Aminothiophenol. **2013**, 3, 2997. https://doi.org/10.1038/srep02997.

(6) Wang, J.; Ando, R. A.; Camargo, P. H. C. Controlling the Selectivity of the Surface Plasmon Resonance Mediated Oxidation of P-Aminothiophenol on Au Nanoparticles by Charge Transfer from UV-Excited TiO_2. *Angew. Chemie - Int. Ed.* **2015**, *54* (23), 6909–6912. https://doi.org/10.1002/anie.201502077.

(7) Zhao, L.B.; Huang, Y.F.; Liu, X.M.; Anema, J. R.; Wu, D.Y.; Ren, B.; Tian, Z.Q. A DFT Study on Photoinduced Surface Catalytic Coupling Reactions on Nanostructured Silver: Selective Formation of Azobenzene Derivatives from Para-Substituted Nitrobenzene and Aniline. *Phys. Chem. Chem. Phys.* **2012**, *14* (37), 12919. https://doi.org/10.1039/c2cp41502j.

(8) Yan, X.; Wang, L.; Tan, X.; Tian, B.; Zhang, J. Surface-Enhanced Raman Spectroscopy Assisted by Radical Capturer for Tracking of Plasmon-Driven Redox Reaction. *Sci. Rep.* **2016**, *6*, 30193. https://doi.org/10.1038/srep30193.

(9) Zhao, Y.; Zhang, Q.; Ma, L.; Song, P.; Xia, L. A p/n Type Silicon Semiconductor Loaded with Silver Nanoparticles Used as a SERS Substrate to Selectively Drive the Coupling Reaction Induced by Surface Plasmons. *Nanoscale Adv.* **2020**, *2* (8), 3460–3466. https://doi.org/10.1039/d0na00350f.

(10) Aditya, T.; Pal, A.; Pal, T. Nitroarene Reduction: A Trusted Model Reaction to Test Nanoparticle Catalysts. *Chem. Commun.* **2015**, *51* (46), 9410–9431. https://doi.org/10.1039/C5CC01131K.

(11) Wang, C. F.; O'Callahan, B. T.; Kurouski, D.; Krayev, A.; El-Khoury, P. Z. The Prevalence of Anions at Plasmonic Nanojunctions: A Closer Look at p-Nitrothiophenol. *J. Phys. Chem. Lett.* **2020**, *11* (10), 3809–3814. https://doi.org/10.1021/acs.jpclett.0c01006.

(12) Almohammed, S.; Zhang, F.; Rodriguez, B. J.; Rice, J. H. Photo-Induced Surface-Enhanced Raman Spectroscopy from a Diphenylalanine Peptide Nanotube-Metal Nanoparticle Template. *Sci. Rep.* **2018**, *8*, 3880. https://doi.org/10.1038/s41598-018-22269-x.

(13) Almohammed, S.; Zhang, F.; Rodriguez, B. J.; Rice, J. H. Electric Field-Induced Chemical SERS Enhancement from Aligned Peptide Nanotube–Graphene Oxide

Templates for Universal Trace Detection of Biomolecules. *J. Phys. Chem. Lett.* **2019**, 10, 1878–1887. https://doi.org/10.1021/acs.jpclett.9b00436.

(14) Krylov, A.; Krylova, S.; Kopyl, S.; Krylov, A.; Salehli, F.; Zelenovskiy, P.; Vtyurin, A.; Kholkin, A. Raman Spectra of Diphenylalanine Microtubes: Polarisation and Temperature Effects. *Crystals* **2020**, *10* (3), 224. https://doi.org/10.3390/cryst10030224.

(15) Sereda, V.; Ralbovsky, N. M.; Vasudev, M. C.; Naik, R. R.; Lednev, I. K. Polarized Raman Spectroscopy for Determining the Orientation of Di-d-Phenylalanine Molecules in a Nanotube. *J. Raman Spectrosc.* **2016**, *47* (9), 1056–1062. https://doi.org/10.1002/jrs.4884.

(16) Handelman, A.; Shalev, G.; Rosenman, G. Symmetry of Bioinspired Short Peptide Nanostructures and Their Basic Physical Properties. *Isr. J. Chem.* **2015**, *55* (6), 637–644. https://doi.org/10.1002/ijch.201400164.